Composites Science and Technology 71 (2011) 39–45

Contents lists available at ScienceDirect

Composites Science and Technology

journal homepage: www.elsevier.com/locate/compscitech

An enhanced FEM model for particle size dependent flow strengthening and interface damage in particle reinforced metal matrix composites

J.C. Shao, B.L. Xiao, Q.Z. Wang, Z.Y. Ma *, K. Yang

Shenyang National Laboratory for Materials Science, Institute of Metal Research, Chinese Academy of Sciences, 72 Wenhua Road, Shenyang 110016, China

ARTICLE INFO

Article history:
Received 17 June 2010
Received in revised form 11 August 2010
Accepted 26 September 2010
Available online 23 October 2010

Keywords:
A. Particle-reinforced composites
B. Debonding
B. Strength
C. Modeling

ABSTRACT

By incorporating the dislocation punched zone model, the Taylor-based nonlocal theory of plasticity, and the cohesive zone model into the axisymmetric unit cell model, an enhanced FEM model is proposed in this paper to investigate the particle size dependent flow strengthening and interface damage in the particle reinforced metal matrix composites. The dislocation punched zone around a particle in the composite matrix is defined to consider the effect of geometrically necessary dislocations developed through a mismatch in the coefficients of the thermal expansion. The Taylor-based nonlocal theory of plasticity is applied to account for the effect of plastic strain gradient which produces geometrically necessary dislocations due to the geometrical mismatch between the matrix and the particle. The cohesive zone model is used to consider the effect of interfacial debonding. Lloyd's experimental data are used to verify this enhanced FEM model. In order to demonstrate flow strengthening mechanisms of the present model, we present the computational results of other different models and evaluate the strengthening effects of those models by comparison. Finally, the limitations of present model are pointed out for further development.

1. Introduction

Particle reinforced metal matrix composites (MMC_P) are of interest for a variety of industrial applications due to their higher stiffness and strength than the matrix alloys. Deep understanding of the strengthening behavior of the MMC_P is a critical issue in development of those materials [1,2]. Experimental observations [1] indicated that the fine particles yielded the increasing strengthening and hardening effects. The continuum models [3,4] based on the classical plasticity theories could explain the load transfer effect from the composite matrix to the reinforcing particle and successfully predict the plastic work hardening behavior of the MMC_P depending on the particle volume fraction and other nondimensional parameters (e.g. particle aspect ratio), but they all failed to explain the particle size dependent strengthening since their constitutive laws possessed no intrinsic material lengths.

In order to explain the particle size effects on the flow strengthening of the MMC_P, a lot of dislocation models have been proposed in the past few decades [5–15]. A number of dislocation punching models [5–10] have been proposed to interpret and predict the observed particle size dependent strengthening of the MMC_P after quenching. Arsenault and Shi [6] proposed a prismatic dislocation punching model to calculate the strengthening which considered the enhanced density of geometrically necessary dislocations (GNDs) resulting from the coefficient of thermal expansion (CTE) mismatch due to quenching. Base on the work of Taya et al. [7], Dunand and Mortensen [8], Shibata et al. [9], and Suh et al. [10] presented an enhanced continuum model for the size dependent strengthening and failure of the MMC_P by defining a CTE mismatch induced GNDs punched zone around the particle and using the cohesive surface model. Except for the dislocation punching models, many researchers introduced particle size effects into the various continuum models by incorporating dislocation plasticity to alter the flow stress in the composite matrix, which achieved good results [11–15]. Nan and Clarke [12] extended the effective medium approach (EMA) by introducing some of the key features of dislocation plasticity into the stress–strain relation of composite matrix. Dai et al. [13] developed a hybrid micromechanical approach by combining the GNDs model with the incremental micromechanical scheme. Tohgo et al. [15] extended the incremental damage model of the MMC_P by introducing the particle size effects using Nan–Clarke's simple method.

Based on the notion of GNDs induced by the geometrical mismatch between the matrix and the particle, strain gradient plasticity theories [16–22] have been developed in order to characterize the particle size dependent strengthening of the MMC_P. Gao et al. [16] proposed a mechanism-based theory of strain gradient plasticity (MSG) to account for the plastic strain gradient in the MMC_P. Gao and Huang [17] developed a Taylor-based nonlocal theory

* Corresponding author. Tel./fax: +86 24 83978908.
E-mail address: zyma@imr.ac.cn (Z.Y. Ma).

0266-3538/$ - see front matter © 2010 Elsevier Ltd. All rights reserved.
doi:10.1016/j.compscitech.2010.09.014

(TNT) of plasticity which was more direct and simple than other gradient plasticity theories. Huang et al. [20] established a conventional theory of mechanism-based strain gradient plasticity (CMSG) to account for particle size effects, and Qu et al. [21] extended the CMSG by including the effects of quenching hardening and accounted for the particle/matrix interfacial debonding via the cohesive zone model.

Based on the summary of previous works, in this paper we consider the following mechanisms responsible for the particle size dependent flow strengthening and interface damage of the MMC_P and construct an enhanced FEM model:

(1) CTE mismatch induced GNDs are not counted as part of the background dislocation density distributed over the entire composite matrix volume but as a dislocation punched zone around the particle;
(2) Taylor-based nonlocal theory of plasticity is used to account for the plastic strain gradient which produces GNDs due to the geometrical mismatch between the matrix and the particle when the MMC_P is plastically deformed;
(3) An axisymmetric unit cell model containing three zones with an imperfect particle/matrix interface (through cohesive zone model) is employed to represent the representative cell of the MMC_P with a regular array of spherical particle.

2. Dislocation strengthening behavior in the MMC_P

It has been proposed by Ashby [5] that there are two possible sources of the GNDs. The first is the CTE mismatch between particle and matrix induced GNDs when the composite is cooled down from the processing temperature. The second is the geometrical mismatch, i.e. it is a result of the deformation-induced plastic strain gradient that arises when the composite is plastically deformed. Here, we consider that the strengthening effects include both the CTE mismatch induced GNDs and the geometrical mismatch induced GNDs as follows.

2.1. Enhancement due to CTE mismatch induced GNDs

In order to illustrate the strengthening effect of CTE mismatch induced GNDs, Taya et al. [7] proposed a dislocation punching mechanism which was schematically illustrated in Fig. 1a–c. According to their theory, the temperature change induced CTE mismatch strain can be represented by arrays of prismatic dislocation loops adhered uniformly to the matrix–particle interface before punching (Fig. 1b). When the thermal stress exceeds the yield strength of the composite matrix, these dislocation loops near the interface are punched out into the composite matrix with a punching distance R to relax the thermal stress and form a dislocation punched zone in the composite matrix, as illustrated in Fig. 1c.

2.1.1. Size of the dislocation punched zone

In order to determine the size of the dislocation punched zone, Shibata et al. [9] calculated the punching distance of the CTE mismatch induced GNDs using a combined plastic energy dissipation and Eshelby theory, accounting for the effect of particle volume fraction. Adopting the approach in Ref. [9], the punching distance R, which stands for the size of the dislocation punched zone from the center of the spherical shape particle, is:

$$R = r\left\{\frac{B(1-2Pf)+\sqrt{B^2(1-2Pf)^2+16(\tau_{ym}/G_m)PB}}{4(\tau_{ym}/G_m)}\right\}^{\frac{1}{3}} \quad (1)$$

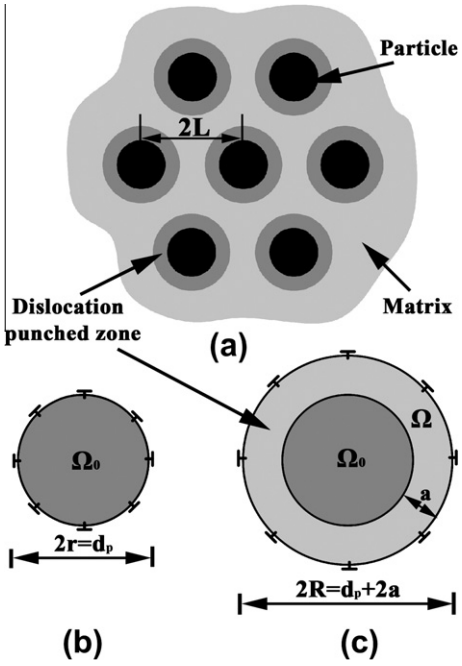

Fig. 1. (a) Schematic illustration of distribution of dislocation punched zones around individual particles [7,10]. (b) CTE mismatch induced arrays of prismatic dislocation loops adhered uniformly to the matrix–particle interface before punching. (c) Punched zone corresponding to equilibrium of punched dislocations after punching.

where f is the particle volume fraction and r is the particle radius. The coefficients B and P are determined from the elastic coefficients and the thermal mismatch as:

$$B = \frac{(1+\nu_m)|\Delta CTE\cdot\Delta T|}{(1-\nu_m)} \quad (2)$$

$$P = \frac{2(1-\nu_m)(3\bar{\lambda}+2\bar{G})}{(1-\nu_m)\{(1-f)(3\bar{\lambda}+2\bar{G})(\frac{1+\nu_m}{1-\nu_m})+3[f(3\lambda_p+2G_p)+(1-f)(3\lambda_m+2G_m)]\}} \quad (3)$$

Here subscripts "m" and "p" stand for the matrix and particle, respectively. In Eqs. (1)–(3), ΔCTE is the difference in the CTE between the matrix and the particle, ΔT is the temperature change, τ_{ym} is the shear yield strength of the matrix, which can be identified as the frictional stress for the glide motion of dislocations, and is assumed to be constant without considering the work hardening effect [9], G is the shear modulus, ν is the Poisson's ratio, and $\bar{\lambda}=\lambda_p-\lambda_m$ and $\bar{G}=G_p-G_m$ are the mismatches of the Lame constants.

It should be noted that there is an upper bound on the punching distance R to be determined geometrically by the condition of $R \leqslant L$ (where $2L$ is the interparticle distance). When the CTE mismatch strain is sufficiently large leading to $R > L$, the dislocation punched zone boundary of a particle touches that of the neighboring particle and the GNDs from a particle annihilate those generated by its neighboring particle. This may be realized in special cases, e.g., a high volume fraction of particle (>20%) or a local-cluster distribution.

2.1.2. Flow strengthening due to dislocation punching

The enhanced density of the CTE mismatch induced GNDs (ρ^{CTE}_{GNDs}) is estimated as the total length of punched prismatic dislocation loops that are needed to relieve the thermal mismatch strain in simple configurations divided by the punched zone volume size a, bounded by an outer radius R (the punching distance calculated

in the previous section) and inner radius r (the particle radius). If we assume that these dislocations are generated homogeneously throughout the punched zone, which has been shown not to be strictly true, and the thermal stress is relieved by the generation of dislocations, the ρ_{GNDs}^{CTE} in the composite matrix due to punching can be written as follows in line with Ref. [8].

$$\rho_{GNDs}^{CTE} = \frac{6\sqrt{2}\Delta CTE \cdot \Delta T \cdot r^2}{b \cdot (R^3 - r^3)} = \frac{12\sqrt{2}\Delta CTE \cdot \Delta T}{b \cdot d_p} \frac{F_p}{1 - F_p} \quad (4)$$

where $F_p = (r/R)^3$ and b is the magnitude of the Burgers vector.

The strengthening of the composite matrix in the punched zone from the CTE mismatch induced GNDs can therefore be estimated according to the Taylor relation [23]:

$$\Delta\sigma_{GNDs}^{CTE} = \alpha G_m b \sqrt{\rho_{GNDs}^{CTE}} \quad (5)$$

where $\alpha = 1.25$ is the Taylor's coefficient for aluminum [24].

2.2. Enhancement due to geometrical mismatch induced GNDs

When the MMC$_P$ is plastically deformed, the geometrical mismatch induced GNDs will be generated in the composite matrix as a result of deformation-induced plastic strain gradient, as shown in Fig. 2. Many mechanism-based strain gradient plasticity theories from the Taylor dislocation model have been applied to investigate the particle size dependent flow strengthening in the MMC$_P$ due to the enhanced density of geometrical mismatch induced GNDs (ρ_{GNDs}^{GM}) and give tensile flow stress σ_{flow} in terms of ρ_{GNDs}^{GM} as follows [16–18,20]:

$$\sigma_{flow} = M\beta G_m b \sqrt{\rho_{SSDs} + \rho_{GNDs}^{GM}} = \sqrt{[\sigma_{ref} f(\varepsilon^p)]^2 + M^2 \bar{r} \beta^2 G_m^2 b \eta^p} \quad (6)$$

where ρ_{SSDs} is the density of statistically stored dislocations (SSDs), M is the Taylor factor, which is about 3.06, β is an empirical coefficient around 0.3, $\bar{r}$ is the Nye-factor around 1.90 [21], ε^p is the plastic strain, $\sigma_{ref} f(\varepsilon^p)$ is the uniaxial stress–strain law of the composite matrix in the absence of strain gradient effects and ρ_{GNDs}^{GM} is expressed in terms of the effective plastic strain gradient η^p. In order to construct a more direct and simple theory and to express the ρ_{GNDs}^{GM} in terms of plastic strain ε^p only, Gao and Huang [17] developed a Taylor-based nonlocal theory (TNT) of plasticity which treated the ρ_{GNDs}^{GM} as a nonlocal variable expressed in terms of an integral average of plastic strain, in which no higher-order strains need to be introduced. A simple representative cell model consisting of a spherical particle of radius r embedded in a matrix layer with the particle volume fraction f in the composite is adopted to characterize the MMC$_P$. According to Ref. [17], the flow stress of the composite matrix considering the geometrical mismatch induced GNDs is given by

$$\sigma_{flow} = \sqrt{[\sigma_{ref} f(\varepsilon^p)]^2 + 27\sqrt{\frac{5}{2}}\beta^2 G_m^2 \frac{b}{r} f^{1/3} \varepsilon^p} \quad (7)$$

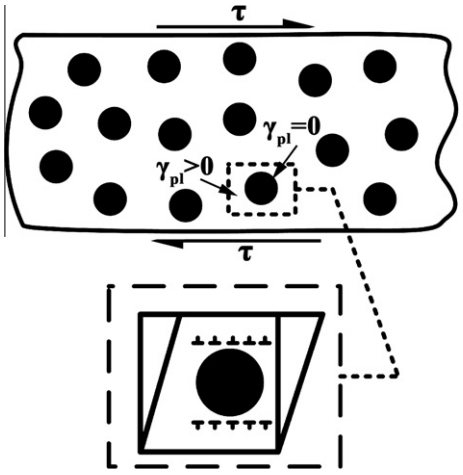

Fig. 2. Plastic strain gradients induced GNDs due to the geometrical mismatch between the particle and the metallic matrix.

3. Enhanced FEM model for MMC$_P$

3.1. Particle/matrix interface model

In order to describe the effect of interfacial debonding on the flow behavior of the MMC$_P$, a cohesive zone model [25,26], which is defined using a traction–separation law instead of considering the presence of a real interphase material, is used. The traction–separation response presently used for the interface is schematically illustrated in Fig. 3, which shows the behavior of both tension and shear on the same axes. The traction–separation response is specified in terms of the critical interface strength, i.e., t_n^0 corresponding to a separation distance of δ_n^0 when the separation is purely normal, and t_s^0 corresponding to a separation distance of δ_s^0 when the separation is tangential, and the work of separation per unit area, i.e., cohesive energy Φ, is equal to the area enclosed by the cohesive curve and the horizontal axis, as shown in Fig. 3. Damage is assumed to initiate when a quadratic interaction function involving the nominal stress ratios, as defined in the expression below, reaches a value of one. This criterion can be represented as

$$\left\{\frac{\langle t_n \rangle}{t_n^0}\right\}^2 + \left\{\frac{t_s}{t_s^0}\right\}^2 = 1 \quad (8)$$

where $\langle\rangle$ are the Macaulay brackets. Under a combination of normal and shear separations across the interface, the effective separation δ_m is defined as

$$\delta_m = \sqrt{\langle \delta_n \rangle^2 + \delta_s^2} \quad (9)$$

The damage evolution which is characterized by a linear degradation of the cohesive stiffness is described through a scalar damage variable D ranging from 0 to 1 that represents a complete loss of the traction at the critical separation distances of δ_n^f and δ_s^f in normal and tangential cases. For linear softening (see Fig. 3) the scalar damage variable D is defined as

$$D = \frac{\delta_m^f(\delta_m^{max} - \delta_m^0)}{\delta_m^{max}(\delta_m^f - \delta_m^0)} \quad (10)$$

where δ_m^{max} refers to the maximum value of the effective displacement attained during the loading history and δ_m^f can be obtained

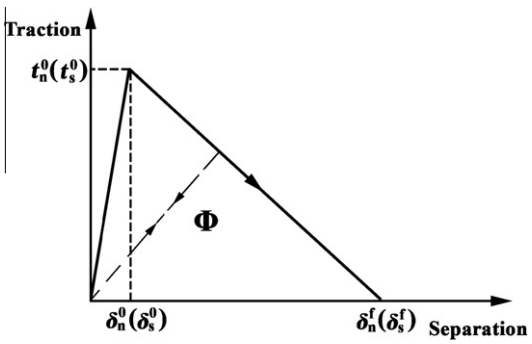

Fig. 3. Traction–separation behavior of the cohesive zone model for the case of interfacial debonding, showing both tension and shear on the same axes.

using the final separations in Eq. (9). And the stress components of the traction–separation law t_n and t_s are affected by the damage variable D and are characterized by a linear degradation of the cohesive stiffness until a complete loss of the traction occurs at the critical separation distances of δ_n^f and δ_s^f according to

$$t_i = \begin{cases} (1-D)\bar{t}_i & \text{if } \bar{t}_i \geqslant 0 \\ \bar{t}_i & \text{otherwise} \end{cases} \tag{11}$$

where $\bar{t}_i$ ($i = n$ or s) are the stress components predicted by the elastic traction–separation behavior for the current separations without damage.

3.2. An axisymmetric unit cell model

We consider a regular array of spherical elastic particle embedded in an elastic–plastic metallic matrix using an axisymmetric unit cell model as the representative cell of the MMC_P (Fig. 4). The unit cell contains three zones: the particle marked by A, the punched zone marked by B and the rest matrix marked by C. The interface between the particle and the matrix is modeled both with and without interfacial debonding. The punched zone size is predicted using Eqs. (1)–(3) and the particle volume fraction f is given by

$$f = \frac{\frac{4\pi}{3}r^3}{\pi L^2 \cdot 2L} = \frac{2r^3}{3L^3} \tag{12}$$

Symmetry boundary conditions are imposed along the x and y axes. An uniform displacement in the positive y direction is prescribed along the top boundary, while the right boundary remains traction-free and straight during deformation. The composite true stress–strain curve of the unit cell is obtained from the reaction force F_y on the cell top surface and the top surface displacement u_y by using the following equations:

$$\bar{\sigma} = \frac{1}{\pi(L')^2}\int_0^{L'} F_y|_{y=L}\,dx \tag{13}$$

$$\bar{\varepsilon} = \ln\left(1 + \frac{u_y}{L}\right) \tag{14}$$

where L is the initial height of the unit cell and L' is the current unit cell radius.

3.3. Material properties of the particle and matrix

In this paper, we use the experimental data from Lloyd [1] for the uniaxial true stress–strain relation of a 15 vol.%SiC_P/A356 composite with two different particle sizes (7.5 and 16 μm) and a thermal quenching ΔT of 474 K. The particle reinforcement is assumed to be isotropic and elastic with Young's modulus $E_p = 427$ GPa, Poisson's ratio $\nu_p = 0.17$ and CTE of $4.3 \times 10^{-6}\,K^{-1}$. The unreinforced matrix is elastic–plastic with Young's modulus $E_m = 76$ GPa, Poisson's ratio $\nu_m = 0.33$, CTE of $23.63 \times 10^{-6}\,K^{-1}$ and the magnitude of the Burgers vector b of 0.28 nm. The uniaxial stress–strain relation of the unreinforced matrix is

$$\sigma_{flow} = \sigma_{ref} f(\varepsilon^p) = \sigma_y\left(1 + \frac{E\varepsilon^p}{\sigma_y}\right)^N \tag{15}$$

where $\sigma_y = 208$ MPa is the yield stress and $N = 0.136$ is the plastic work hardening exponent based on the experimental data in the literature [1].

It is well known that the microstructure and mechanical properties of the composite matrix may be significantly different from those of the unreinforced matrix. In order to model the mechanical behavior of the composite matrix, the flow strengthening effects which are induced by the enhanced dislocation density in the composite matrix due to both CTE mismatch and geometrical mismatch should be considered. As shown in Fig. 4, the composite matrix is divided into two different zones marked by B and C, respectively. For zone B with a limited size a, the dislocation density increasing due to both the CTE mismatch and the geometrical mismatch is considered. Accepting the assumption that the CTE mismatch induced GNDs are homogeneously distributed throughout zone B, we replace $\sigma_{ref} f(\varepsilon^p)$ in Eq. (7) with $\sigma_{ref} f(\varepsilon^p) + \Delta\sigma_{GNDs}^{CTE}$, then the flow stress of the composite matrix in zone B is given by

$$\sigma_{flow} = \sqrt{[\sigma_{ref} f(\varepsilon^p) + \Delta\sigma_{GNDs}^{CTE}]^2 + 27\sqrt{\frac{5}{2}}\beta^2 G_m^2 \frac{b}{r} f^{1/3}\varepsilon^p} \tag{16}$$

For zone C, the dislocation density increasing due to the geometrical mismatch is considered only and the flow stress of the composite matrix in zone C is given by Eqs. (7) and (15).

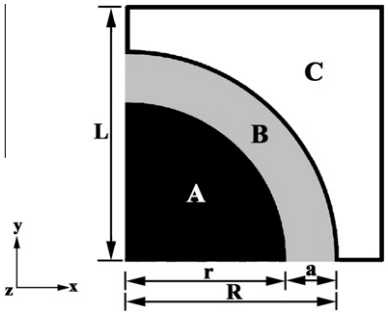

Fig. 4. Schematic diagram of an axisymmetric unit cell model divided into three different zones marked by A, B and C, respectively.

4. Computational results and discussion

First, we discuss the size of the dislocation punched zone resulting from punching of the CTE mismatch induced GNDs in the present study. Second, we use Lloyd's experimental data to verify the proposed enhanced FEM unit cell model. Third, we present the computational results of other different models and evaluate the strengthening effects of these models by comparison. Finally, we discuss the limitations of the present enhanced FEM model.

4.1. The punched zone size of the present model

As seen in Eqs. (1)–(3), many factors affect the punching distance R. In this section, we mainly discuss the effects of the particle radius r and the particle volume fraction f on the punched zone size.

It is obvious that the punching distance R is an increasing function of the particle radius r for the same particle volume fraction f according to Eq. (1). However the value of the punching distance R normalized by the particle radius r is identical for the same particle volume fraction. Thus the ρ_{GNDs}^{CTE} in the composite matrix due to punching decreases as the r increases according to Eq. (4). This predicting trend is in accordance with the experimental results in Refs. [27,28] that the dislocation density decreases as the particle size increases.

The punching distance R also depends on the particle volume fraction f. In Fig. 5, the value of the punching distance R normalized by the particle radius r is plotted against the particle volume fraction f for the SiC_P/A356 composite. By comparison, the value of interparticle spacing L (the side length of the axisymmetric unit cell model) normalized by the particle radius r is also plotted against the particle volume fraction f. As the particle volume fraction f increases, the punching distance R slightly decreases. As

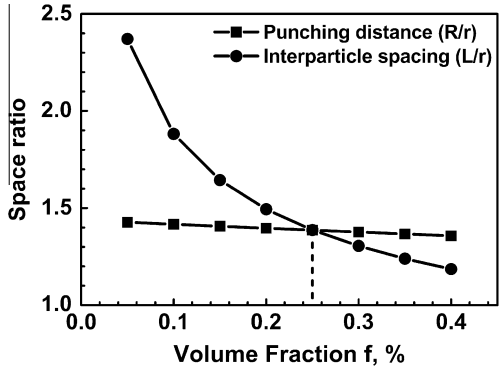

Fig. 5. Variation of the punching distance R and interparticle spacing L normalized by the particle radius r with the particle volume fraction f.

shown in Fig. 5, there is an upper bound on the punching distance R to be determined by the intersection point of these two curves. When the volume fraction f is higher than 25%, the dislocation punched zone of a particle will touch that of a neighboring particle and Eqs. (1)–(4) may be inapplicable. In Lloyd's experiment, the volume fraction f is 15% and so Eqs. (1)–(4) are suitable here.

4.2. Verification of the present enhanced FEM model

In order to verify the present enhanced FEM model, Lloyd's experimental data for the uniaxial true stress–strain relation of the 15 vol.%SiC_P/A356 composite with two different particle sizes (7.5 and 16 μm) under T6 condition is used. Fig. 6a shows the computational results predicted by the present model, neglecting the interfacial debonding. Both the elastic modulus E_c and the yield stress σ_{yc} of the composite agree well with the experimental data. However, the computational results for both particle sizes are consistent with the experimental data only at small strain (less than 2%). As the strain increases, the computational results become much larger than the experimental data because the damage occurs in the composite but is not considered here. The cohesive zone model for the particle/matrix interface discussed in Section 3.1 is used to investigate the interfacial debonding of the MMC_P. The selection of interface parameters is difficult due to the lack of experimental data on the SiC_P/Al interface. In order to choose a representative set of interface parameters to describe the interface behavior, our computational results for the overall stress–strain curve of the 15 vol.%SiC_P/A356 composite containing 7.5 μm diameter SiC particles are fitted to the experimental stress–strain curve. The fitted parameters of $t_n^0 = 350$ MPa, $t_s^0 = 301$ MPa and cohesive energy $\Phi = 56$ J/m^2 have a higher accuracy. These parameters are certainly not unique, but we choose them as a representative set to describe the interface behavior and use them as the interface parameters of the composite containing 16 μm diameter particles.

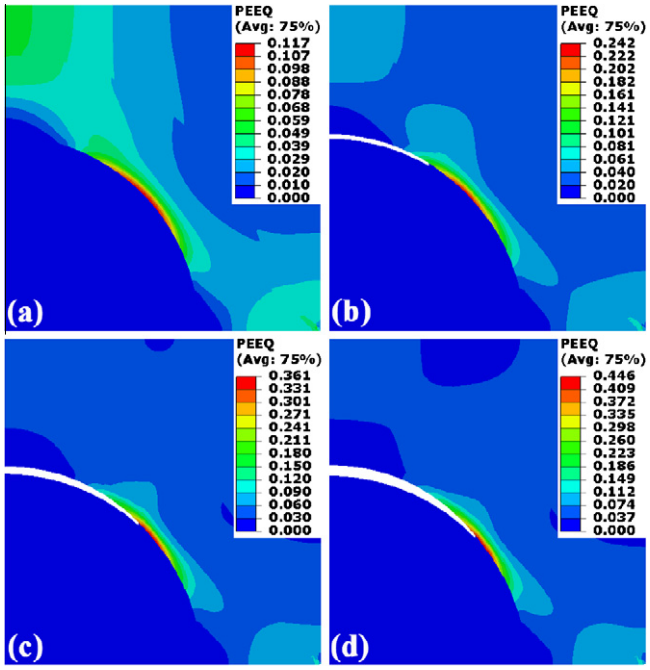

Fig. 7. Counters of equivalent plastic strain $\bar{\varepsilon}$ for the model containing 16 μm SiC_P with imperfect interface at different remote strains: (a) 0.02, (b) 0.03, (c) 0.04 and (d) 0.05.

Counters of equivalent plastic strain $\bar{\varepsilon}$ at different remote strains of 0.02, 0.03, 0.04 and 0.05 are given in Fig. 7, showing the processes of deformation and interfacial debonding for the present enhanced FEM model containing a spherical particle with a size of 16 μm under tensile loading. At a small strain ($\bar{\varepsilon} = 0.02$), as shown in Fig. 7a, the maximum strain concentration occurs at the location 45° from the tensile axis, and no debonding is found along the interface. When the deformation is further developed (Fig. 7b–d), the magnitudes of the strain concentration increase and a small debonding is found along the upper half interface, which propagates from the left to the right along the interface. Due to the symmetry boundary condition used in the axisymmetric unit cell model, no debonding occurs at the point on the symmetry plane, i.e., the x-axis corner of the interface. However, in the real composite, full debonding of the particle/matrix interface is certainly possible.

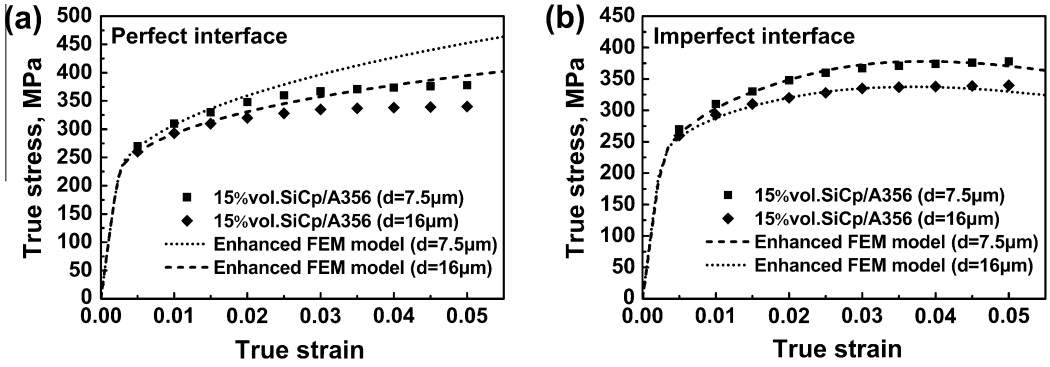

Fig. 6. Comparison between the experimental data reported by Lloyd [1] for 15 vol.%SiC_P/A356 with two different particle sizes and the predicted computational results using the enhanced FEM model: (a) perfect interface and (b) imperfect interface.

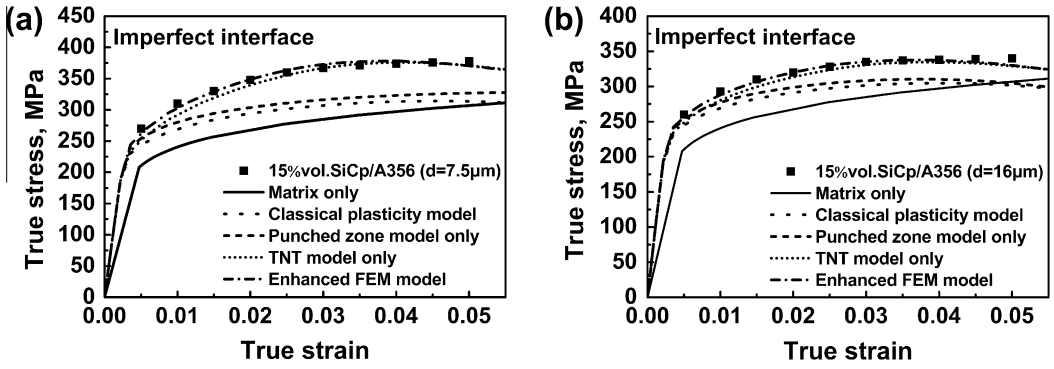

Fig. 8. Comparison between the experimental data and the computational results of different models with imperfect interface corresponding to the classical plasticity model, the punched zone model only, the TNT model only and the present enhanced FEM model: (a) 7.5 μm SiC and (b) 16 μm SiC.

Similar work has been done by Qu et al. [21], who extended the CMSG by including the effects of quenching hardening and assuming that the CTE mismatch induced GNDs were distributed over the entire matrix using Arsenault–Shi's model [6]. By comparison, the present enhanced FEM model gives more detailed descriptions of the CTE mismatch induced GNDs using the punched zone model. Moreover, instead of the CMSG the present enhanced FEM model uses a more direct and simple TNT model, which easily allows the use of readily available finite element software. From Fig. 6b we can see that the predicted tensile true stress–strain curves by the enhanced FEM model agree well with Lloyd's experimental data over the entire range of strain. Therefore, the present enhanced FEM model can well describe the particle size dependent flow strengthening and interface damage of the MMC_P.

4.3. Comparison of different models

The results of different models accounting for the strengthening effects in the MMC_P, using the classical plasticity theory considering the load transfer effect from the metal matrix to the reinforcing particle only, the punched zone model considering the CTE mismatch induced GNDs only, the TNT model considering the geometrical mismatch induced GNDs only, and the present enhanced FEM model including both dislocation punched zone and TNT model, respectively, are shown in Fig. 8a and b. We can see that all these models give the same elastic modulus around $E_c = 94$ GPa of the composite, which agree very well with Lloyd's experimental data. At the same time, the elastic modulus E_c of the composites for 7.5 and 16 μm particle sizes is identical according to the computational results. This result corresponds with the Halpin–Tsai equation [1] and shows that elastic modulus of the composites is mainly determined by the volume fraction of particle and is independent of the particle size.

As demonstrated in Fig. 8a and b, the predicted composite responses using the classical plasticity theory are lower than the experimental data and the strengthening effect with both particle sizes provides the same action. This illustrates the fact that the classical plasticity cannot show the particle size effect. The predicted yield strength according to the enhanced FEM model is more accurate than the classical plasticity model and the TNT model because the latter two models do not consider the strengthening effect due to the CTE mismatch induced GNDs which is the dominant contribution to the yield strength. The punched zone model can describe appropriately the strengthening and particle size effect at low strains (less than 0.5%), but cannot explain the particle size effect observed in Lloyd's experiments that the gap between the true stress–strain curves for 7.5 and 16 μm diameter particles increased with the strain. By comparison, the TNT model can give a better description of the particle size dependent strengthening at large strains. The reason is that the geometrical mismatch induced GNDs is unlikely significant at small plastic strains, but it is the source of strengthening contribution at large strains. As the strain increases, the interfacial debonding occurs and the rate of strain hardening due to geometrical mismatch induced GNDs decreases. Then the predicted stress–strain curves become softening after the peaks.

To sum up, the present enhanced FEM model integrates the advantages of the classical plasticity theory model, punched zone model, TNT model and interfacial debonding model, and can be used to interpret and predict the particle size dependent flow strengthening and interface damage in the MMC_P.

4.4. Limitations of the present enhanced FEM model

(1) We assume that particles are regularly distributed in the MMC_P and use an axisymmetric unit cell model containing one particle to represent the whole composite. But in the real MMC_P, the particles are usually distributed randomly and sometimes are congregated. This unit cell model containing one particle could not analyze the effect of particles distribution on the mechanical behavior of the MMC_P.
(2) The real particles usually have irregular shapes but the particle is assumed to be spherical in this paper for simplifying the calculation.
(3) The three basic failure mechanisms in the MMC_P are brittle cracking of the particles, decohesion at the interface between particle/matrix, and ductile failure of the matrix. In this paper, we ignore the failure mechanisms of brittle cracking of the particles and ductile failure of the matrix and only consider the effect of interfacial debonding.

5. Conclusions

By incorporating the dislocation strengthening effect and interface damage criterion into an axisymmetric unit cell model, we develop an enhanced FEM model for characterizing the particle size dependent flow strengthening and interface damage in the MMC_P. In the present enhanced FEM model, direct strengthening (classical plasticity considering the load transfer effect through FEM model), indirect strengthening (CTE mismatch and geometrical mismatch induced GNDs), and interfacial debonding effects (cohesive zone model) are incorporated. Comparisons with the experimental data and other different models demonstrate that the present enhanced FEM model can well describe the particle size dependent flow strengthening and interface damage of the MMC_P.

References

[1] Lloyd DJ. Particle reinforced aluminum and magnesium matrix composites. Int Mater Rev 1994;39:1–23.
[2] Chawla N, Andres C, Jones JW, Allison JE. Effect of SiC volume fraction and particle size on the fatigue resistance of a 2080 Al/SiC_P composite. Metall Mater Trans A 1998;29:2843–54.
[3] Voituriez C, Hall IW. Strengthening mechanisms in whisker-reinforced aluminum composites. J Mater Sci 1991;26:4241–9.
[4] Wu Y, Lavernia EJ. Strengthening behavior of particulate reinforced MMCs. Scripta Mater 1992;27:173–8.
[5] Ashby MF. The deformation of plasticity non-homogeneous materials. Philos Mag 1970;21:399–424.
[6] Arsenault RJ, Shi N. Dislocation generation due to differences between the coefficients of thermal expansion. Mater Sci Eng A 1986;81:175–87.
[7] Taya M, Lulay KE, Lloyd DJ. Strengthening of a particulate metal matrix composite by quenching. Acta Metall Mater 1991;39:73–87.
[8] Dunand DC, Mortensen A. On plastic relaxation of thermal stresses in reinforced metals. Acta Metall Mater 1991;39:127–39.
[9] Shibata S, Taya M, Mori T, Mura T. Dislocation punching from spherical inclusions in a metal matrix composite. Acta Metall Mater 1992;40:3141–8.
[10] Suh YS, Joshi SP, Ramesh KT. An enhanced continuum model for size-dependent strengthening and failure of particle-reinforced composites. Acta Mater 2009;57:5848–61.
[11] Miller WS, Humphreys FJ. Strengthening mechanisms in particulate metal matrix composites. Scripta Mater 1991;25:33–8.
[12] Nan CW, Clarke DR. The influence of particle size and particle fracture on the elastic/plastic deformation of metal matrix composites. Acta Mater 1996;44:3701–811.
[13] Dai LH, Ling Z, Bai YL. Size-dependent inelastic behavior of particle-reinforced metal–matrix composites. Compos Sci Technol 2001;61:1057–63.
[14] Trojanová Z, Drozd Z, Kúdela S, Száraz Z, Lukáč P. Strengthening in Mg–Li matrix composites. Compos Sci Technol 2007;67:1965–73.
[15] Tohgo K, Itoh Y, Shimamura Y. A constitutive model of particulate-reinforced composites taking account of particle size effects and damage evolution. Composites A 2010;41:313–21.
[16] Gao H, Huang Y, Nix WD. Mechanism-based strain gradient plasticity – I. Theory. J Mech Phys Solids 1999;47:1239–63.
[17] Gao H, Huang Y. Taylor-based nonlocal theory of plasticity. Int J Solids Struct 2001;38:2615–37.
[18] Xue Z, Huang Y, Li M. Particle size effect in metallic materials: a study by the theory of mechanism-based strain gradient plasticity. Acta Mater 2002;50:149–60.
[19] Liu LF, Dai LH, Yang GW. Strain gradient effects on deformation strengthening behavior of particle reinforced metal matrix composites. Mater Sci Eng A 2003;345:190–6.
[20] Huang Y, Qu S, Hwang KC, Li M, Gao H. A conventional theory of mechanism-based strain gradient plasticity. Int J Plast 2004;20:753–82.
[21] Qu S, Siegmund T, Huang Y, Wu PD, Zhang F, Hwang KC. A study of particle size effect and interface fracture in aluminum alloy composite via an extended conventional theory of mechanism-based strain-gradient plasticity. Compos Sci Technol 2005;65:1244–53.
[22] Yan YW, Geng L, Li AB. Experimental and numerical studies of the effect of particle size on the deformation behavior of the metal matrix composites. Mater Sci Eng A 2007;448:315–25.
[23] Taylor GI. The mechanism of plastic deformation of crystals. Part 1. Theoretical. Proc Roy Soc Lond A 1934;145:362–87.
[24] Hansen N. The effect of grain size and strain on the tensile flow stress of aluminum at room temperature. Acta Metall 1977;25:863–9.
[25] Zhang H, Ramesh KT, Chin ESC. Effects of interfacial debonding on the rate-dependent response of metal matrix composites. Acta Mater 2005;53:4687–700.
[26] Abaqus. Abaqus user manual. Version 6.8.
[27] Arsenault RJ, Wang L, Feng CR. Strengthening of composites due to microstructural changes in the matrix. Acta Metall Mater 1991;39:47–57.
[28] Clyne TW, Withers PJ. An introduction to metal matrix composites. Cambridge: Cambridge University Press; 1993.